Raytracing with MARX — X-ray observatory design, calibration, and support

John E. Davis[a], Mark W. Bautz[a], Daniel Dewey[a], Ralf K. Heilmann[a], John C. Houck[a], David P. Huenemoerder[a], Herman L. Marshall[a], Michael A. Nowak[a], Mark L. Schattenburg[a], Norbert S. Schulz[a], Randall Smith[b]

[a]MIT Kavli Institute for Astrophysics, Cambridge MA. USA;
[b]Smithsonian Astrophysical Observatory, Cambridge MA, USA

ABSTRACT

MARX is a portable ray-trace program that was originally developed to simulate event data from the transmission grating spectrometers on-board the Chandra X-ray Observatory (CXO). **MARX** has since evolved to include detailed models of all CXO science instruments and has been further modified to serve as an event simulator for future X-ray observatory design concepts.

We first review a number of CXO applications of **MARX** to demonstrate the roles such a program could play throughout the life of a mission, including its design and calibration, the production of input data products for the development of the various software pipelines, and for observer proposal planning.

We describe how **MARX** was utilized in the design of a proposed future X-ray spectroscopy mission called ÆGIS (Astrophysics Experiment for Grating and Imaging Spectroscopy), a mission concept optimized for the 0.2 to 1 keV soft X-ray band. ÆGIS consists of six independent Critical Angle Transmission Grating Spectrometers (CATGS) arranged to provide a resolving power of 3000 and an effective area exceeding 1000 cm^2 across its passband. Such high spectral resolution and effective area will permit ÆGIS to address many astrophysics questions including those that pertain to the evolution of Large Scale Structure of the universe, and the behavior of matter at very high densities.

The **MARX** ray-trace of the ÆGIS spectrometer yields quantitative estimates of how the spectrometer's performance is affected by misalignments between the various system elements, and by deviations of those elements from their idealized geometry. From this information, we are able to make the appropriate design tradeoffs to maximize the performance of the system.

Keywords: Marx, X-Ray, Ray-Trace, AEGIS

1. INTRODUCTION

The Chandra end-to-end science simulator, Model of AXAF Response to X-rays (**MARX**),[1] is a portable ray-trace program that is capable of producing detailed and realistic simulations of Chandra X-ray Observatory[2,3] observations of X-ray sources. The original motivation for **MARX** was to provide simulated event data for the development and testing of algorithms for the Chandra grating data processing software. Over time the simulator has evolved to include detailed models of the Chandra mirrors, focal plane detectors, and diffraction gratings. It is now used routinely to facilitate proposal planning, to aid in the calibration of science instruments,[4] for algorithm development and construction of realistic test data.[5]

Recently, **MARX** has played an increasingly important role in the development of new X-ray mission concepts. It has been used to study the various aberrations from different Rowland torus configurations for the Critical Angle Transmission Grating Spectrometer[6] (CATGS) proposed for the International X-ray Observatory[7] (IXO), Advanced X-ray Spectroscopic Imaging Observatory[8] (AXSIO), and Astrophysics Experiment for Grating and Imaging Spectroscopy[9] (ÆGIS). By including other important sources of aberrations such as mirror

Further author information: (Send correspondence to J.E.D.)
J.E.D.: E-mail: davis@space.mit.edu

Space Telescopes and Instrumentation 2012: Ultraviolet to Gamma Ray,
edited by Tadayuki Takahashi, Stephen S. Murray, Jan-Willem A. den Herder,
Proc. of SPIE Vol. 8443, 84431A · © 2012 SPIE · CCC code: 0277-786/12/$18 · doi: 10.1117/12.926937

misalignments, finite grating facet sizes, astigmatic effects, and so on, we have been able to make realistic predictions of the resolving power of the grating spectrometers. Looking farther down the road beyond the design stage, we expect **MARX** to play a continuing role in these missions just as it has for Chandra.

In the next section we give a summary of the basic **MARX** usage to help the reader understand the sections that follow. We will also discuss those aspects of the **MARX** architecture that have been important in adapting **MARX** to other missions. In the third section, we present some examples of the use of **MARX** for Chandra calibration and proposal planning. We then show how **MARX** has been used for the exploration of future X-ray mission concepts, in the context of the ÆGIS proposal. We start by presenting some details of the ÆGIS design in section 4 and then in section 5 we show some of the ways that **MARX** has been used to refine the design. A brief summary follows in section 6.

2. AN OVERVIEW OF MARX

In this section, we give an overview of **MARX** for those that are unfamiliar with it. We refer the reader to the **MARX** web page* for more detailed information.

2.1 Features

MARX is a rather complete end-to-end science simulator for Chandra X-ray Observatory that enables the user to produce simulated events for a wide variety of astrophysical X-ray sources. It contains support for all of the scientific instruments on-board the spacecraft including detailed models for the High Resolution Mirror Assembly (HRMA), the Low and High Energy Transmission Gratings[10] (LETG and HETG), the Advanced CCD Imaging Spectrometer (ACIS), the High Resolution Imaging and Spectroscopic Cameras (HRC-I/S), as well as the little known HRC-S High Energy Suppression Filter (HESF). While **MARX** does not explicitly support the Aspect Camera System, it does include support for spacecraft dither via an internal dither model or through the use of observation-specific Pointing, Control and Attitude Determination (PCAD) files. Each year **MARX** is updated to maintain consistency with the most recent calibration for each of the supported instruments.

2.2 Components

MARX is a suite of several programs that together are capable of producing simulated Chandra event lists and aspect solution files.

The most important program in the suite is called `marx`. It is the program that actually performs the raytrace and writes the results to a set of files in a native **MARX** format. In this paper, we shall refer to the files in this format as the "marx vectors".

The `marx2fits` program may be used to convert the marx vectors into a standard Chandra event file in the Flexible Image Transport System (FITS) format for subsequent processing by the Chandra Interactive Analysis of Observations (**CIAO**) software†. The **MARX** distribution also includes some code for the **IDL** and **S-Lang**‡ interpreters that may be used for reading the raw marx vectors.

The `marxasp` program may be used to construct the corresponding Chandra aspect solution file for use by those **CIAO** tools that require it.

The `marxpileup` program may be used to simulate the effects of pileup[11] for those observations where pileup in the ACIS detector is a concern.

2.3 Implementation

The programs are written entirely in ANSI C and have been used on numerous 32- and 64-bit flavors of Unix (Linux, Solaris, OpenBSD, NetBSD, ...), MacOSX, and on Windows (via cygwin). With the exception of an ANSI compatible C compiler (such as `gcc`) and a C library, no external dependencies are required to build and use the software. The source code is freely available from the **MARX** web site, and is distributed under the terms of the GNU General Public License (version 2).

*`http://space.mit.edu/cxc/marx/`

†`http://cxc.harvard.edu/ciao/`

‡`http://www.jedsoft.org/slang/`

2.4 Running MARX

`Marx` uses an Image Reduction and Analysis Facility (IRAF) style parameter interface, which is a widely used paradigm in the X-ray astrophysics data analysis community. A typical simulation requires only a few parameters to be specified. For example, a 30 ksec HETG/ACIS-S simulation of an on-axis point source may be created using

```
marx SourceType=POINT ExposureTime=30000 DetectorType=ACIS-S GratingType=HETG \
   SourceRA=0 SourceDEC=0 RA_Nom=0 Dec_Nom=0 Roll_Nom=0 \
   MinEnergy=0.5 MaxEnergy=7 SourceFlux=0.001 OutputDir=point
```

For this example, a point source with a flat energy spectrum (from 0.5 to 7 keV) and an integrated flux of 0.001 photons/sec/cm^2 was assumed. `Marx` also supports an arbitrary spectral shape via the `SpectralFile` parameter; this feature is used in the examples presented in section 3.

When `marx` runs, it first collects a number of photons (or "rays") from the source object. It is the responsibility of the source to assign each of the rays a time, direction and energy value. Most users of `marx` use one of its built-in sources (`POINT`, `IMAGE`, ...), but for maximum flexibility, `marx` also allows the user to create custom source objects that are dynamically loaded into `marx` at run-time. The simulation of the Galactic center described in the next section used this technique.

The rays from the source are then projected to the opening aperture of a mirror object and raytraced through the mirror. If the telescope is dithering, the direction of the ray at the aperture will be modified by the instantaneous orientation of the telescope. Rays that get absorbed or do not reflect are discarded. For Chandra, the mirror object is `HRMA`, which implements the appropriate Wolter-I geometry and incorporates the known misalignments of the Chandra mirrors. It uses iridium optical constants to compute the reflection probability, which is a function of both grazing angle and energy.

Rays that make it through the optic are then projected to a grating object, which is `HETG`, `LETG`, or `NONE` for Chandra simulations. The diffraction probability into a particular diffraction order is given by the appropriate diffraction efficiency file. The direction of the diffracted ray is computed from the 3-d version of the grating equation that properly accounts for the orientation of the incoming ray with respect to the grating facet. For Chandra simulations, the effects of finite facet size and period errors are treated statistically. Grating misalignments are looked up in a grating misalignment file.

From the grating object, rays are propagated to the detector object where each is assigned a detector coordinate and pulse-height. The energy-dependent detection probability for those rays that hit the detector is looked up in a detector-specific efficiency file. For Chandra, the standard focal plane detector objects are `ACIS-I`, `ACIS-S`, `HRC-I`, and `HRC-S`.

Hence, input rays originate at a source and propagate sequentially from a mirror object where focussing occurs, to a grating object, where diffraction takes place, and on to a detector object, where the ray becomes an "event", either detected or undetected. `Marx` repeats this cycle until the specified stopping criteria has been met, e.g., the specified exposure time has elapsed.

Once the simulation is complete, the next step is to convert the marx vectors into the form of a Chandra level-2 events file through the use of the `marx2fits` program. Optional steps include running the pileup simulator `marxpileup` and the creation of an aspect solution file with `marxasp`. From this point one can extract Pulse Height Analysis (PHA) histograms and create matching effective area files (ARFs)[12] via the CIAO tools for analysis in a spectral modeling program such as **ISIS**[13§].

3. CHANDRA EXAMPLES

The examples presented in this section were chosen to illustrate the power and flexibility of **MARX**. We refer the user to the **MARX** web page for examples that are more tutorial in nature.

[§] `http://space.mit.edu/cxc/isis/`

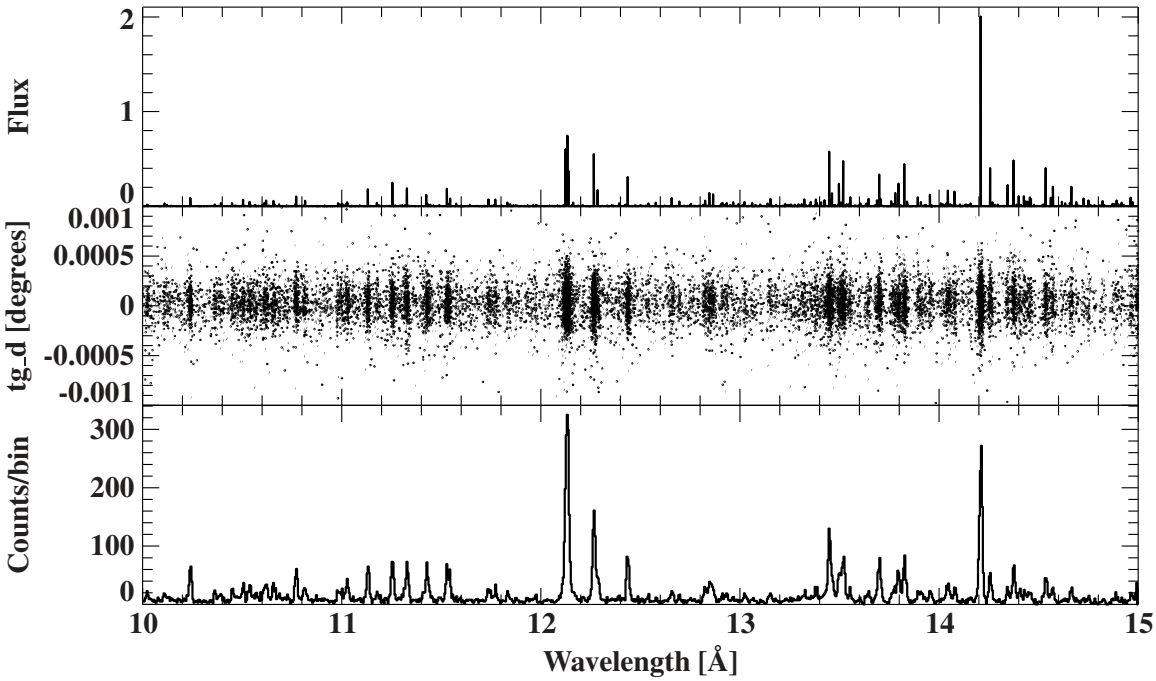

Figure 1. A simulation of the Capella X-ray coronal plasm using the HETG and the ACIS-S detector. The input spectrum, shown in the top panel, was created using the APED model in **ISIS**. The middle panel shows the simulated events for a selected wavelength range in diffraction coordinates and the bottom represents the corresponding counts histogram.

3.1 Capella

Most proposal planning uses of **MARX** require the user to generate a text file that specifies the energy spectrum that is expected to enter the aperture of the telescope. This file consists of two columns: an energy column, and a flux column representing the flux density at that energy. We illustrate this usage in the context of Capella, which is a binary star system consisting of two cool giant stars, a type G1 III star and a slightly more massive type G8 III star. The latter star is believed[14] to be the dominant source of the X-ray coronal emission with a plasma temperature of about 10^7 K.

To simulate what one would expect from a 40 ksec HETGS observation of Capella, we used **ISIS** to generate a spectral file¶ from a model that utilizes the Astrophysical Plasma Emission Database (APED), which describes a thermal plasma in collisional ionization equilibrium. A plot of a portion of the input spectrum and simulated first-order events in the MEG grating is shown in Figure 1. The broadening that is seen in the extracted spectrum is due a combination of effects, including the intrinsic blur of the Chandra mirrors, finite grating facet sizes, grating period errors, detector pixelation effects, aspect reconstruction uncertainties, and various system misalignments. We point out that **MARX** has been calibrated[15] to reproduce the broadening of the line profiles that is seen in real Chandra data.

3.2 PSF Calibration

MARX has become an important link in the tool chain used for the calibration of the Chandra Point Spread Function (PSF), where it is used to project simulated rays from **SAOTrace**,[16] the high fidelity HRMA mirror model, to the detector for comparison with flight data. Used in this way, **SAOTrace** simply becomes a source

¶A script (`marxflux`) to create properly a formatted spectral file for an arbitrary "xspec" model is included in the **MARX** distribution.

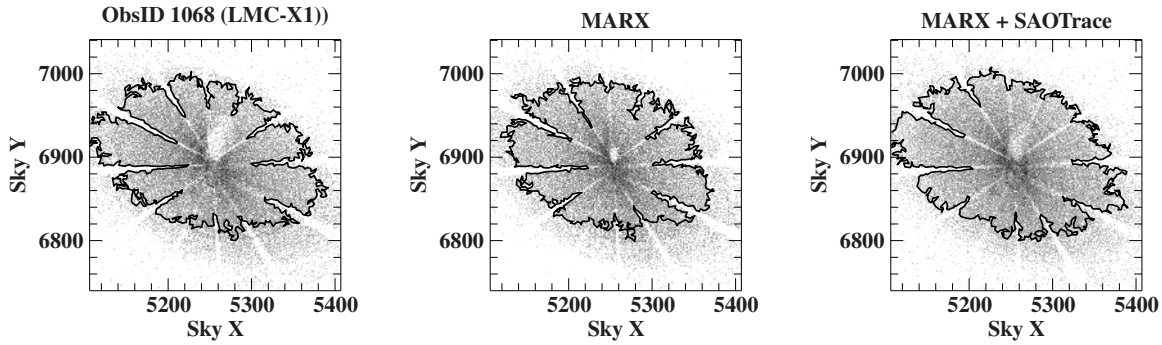

Figure 2. Figure comparing the **MARX**-simulated PSF with that of real data. The plot on the left is a Chandra image of LMC-X1 viewed 25 arc-minutes off-axis by ACIS-S. The image in the middle is a pure **MARX** simulation of the source, and the one on the right is a **MARX** simulation using the SAOTrace mirror model. The dark curve on each of the images represents the 95 percent encircled energy contour.

for **MARX** rays and the **MARX** mirror model is bypassed. Support for **SAOTrace** rays is also important for the analysis of those observations that require a higher fidelity mirror model than the one built into **MARX**. For example, one might prefer to use **SAOTrace** rays to help decide whether an off-axis PSF is due to a point source, or one that is extended.

The difference between the **MARX** and **SAOTrace** mirrors is shown in Figure 2, which compares the **MARX** and **SAOTrace** PSFs to that of a 25 arc-minute off-axis Chandra observation of LMC-X1 (ObsID 1068). In these simulations, a point source was placed 25 arc-minutes off-axis with the aimpoint on ACIS-I and events detected on ACIS-S. While rather large differences between **MARX** and **SAOTrace** can be seen in the core of the PSF, the 95 percent encircled energy contours are in reasonable agreement.

3.3 Galactic Center

Sagittarius A* is a bright radio source that lies at the center of our galaxy and is believed to be a supermassive black hole. While there have been a number of Chandra imaging observations of Sgr A*, until recently there have been no grating observations. In this section, we describe the **MARX** simulations that were used (successfully) to argue that a 3 megasecond HETG/ACIS-S observation would be scientifically worthwhile.

The **MARX** simulations of the Galactic center were based on the data from Chandra ObsID 3392, a 170 ksec ACIS-I observation of Sgr A*. Data from this observation is shown in the left image of Figure 3. As can been seen from this figure, many other X-ray sources are located near Sgr A*, and there is substantial emission from the nebula surrounding it. As such, the simulation could not treat Sgr A* as an isolated point source, but had to take into account all of the emission in its vicinity. This required the creation of a custom source model, which in **MARX** parlance is called a "user-source", that gets dynamically linked into `marx` during run-time.

A **S-Lang** module was developed to compute a spatial probability density function for the galactic center utilizing the Delaunay Tessellation Field Estimator methodology.[17] The locations of all of the level-2 events from ObsID 3392 were used as vertices for the triangulation. Then the probability distribution was exposure corrected via a time-weighted exposure map. In part, this had the effect of removing the chip gaps that can been seen in the ACIS-I image of the observed data on the left in Figure 3. A **MARX** user-source module containing an instance of the **S-Lang** interpreter was used to sample source positions from the spatial density map. The sampled locations were used to determine ray positions and directions. The energy assigned to a given ray was determined by sampling from a Gaussian distribution of energies whose sigma and mean were determined by the event from ObsID 3392 closest to the ray position. For positions within 1.5 arc-seconds of Sgr A*, the energies were sampled from a spectrum of an absorbed continuum and iron lines consistent with the quiescent ACIS-I spectrum of Sgr A*.

An image of the resulting simulation is shown on the right in Figure 3. Note that the ACIS-I chip gaps can no longer be seen, and in their place is an ACIS-S chip gap. One can also make out the diffracted events from

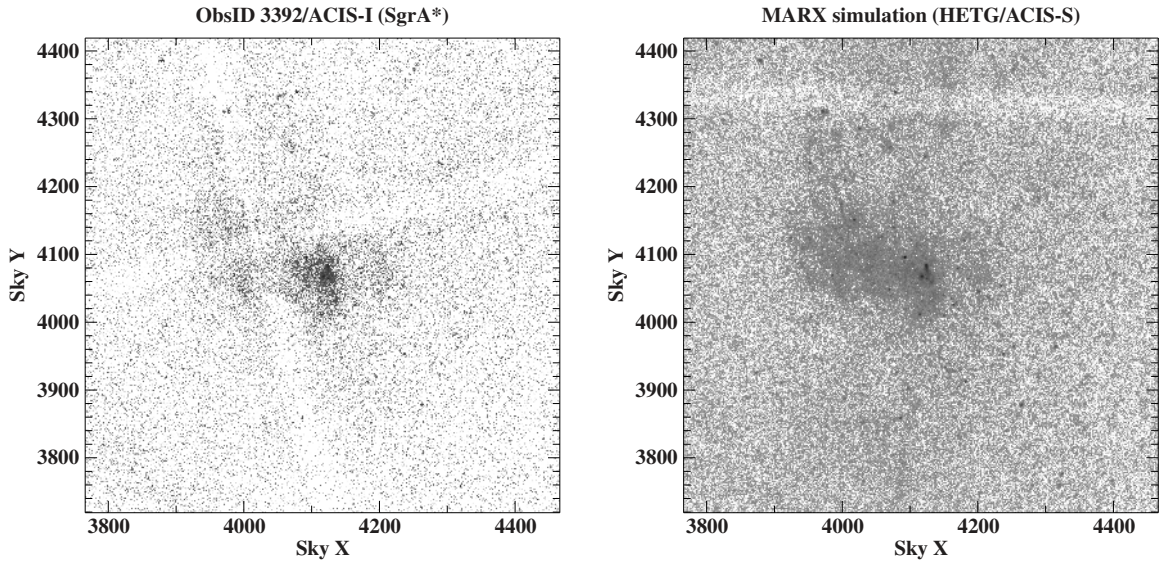

Figure 3. The image on the left was produced from from a 167 ksec exposure in 2002 of the Galactic center using Chandra's ACIS-I CCD camera with a roll angle of 75 degrees (ObsID 3392). Sagittarius A* is one of the bright objects in the center of this image. The image on the right is a 3 Msec HETG+ACIS-S simulation of the Galactic center using a 92 degree roll angle based on the event data from ObsID 3392. The light horizontal band near the top of the image on the right is caused by the chip gap between two of the ACIS-S chips. The slightly tilted vertical line on this image is due to the diffracted photons from the central region where SgrA* is located. The increased count density of the simulated data is due to its much longer exposure time.

the emission near Sgr A*, as well as sources that fall very near the dispersion curve. **MARX** simulations were also used to identify a set of observing roll angles that minimize contamination from sources along the dispersion curve.

4. THE ÆGIS MISSION CONCEPT

ÆGIS originated as a response to the NASA 2011 *Request for Information Concepts* for its next X-ray astronomy mission. It was designed to be a moderate cost soft X-ray spectrometer with an effective area greater than 1000 cm^2 and a resolving power in excess of 3000 across the 0.3 to 1 keV energy band. A summary of its expected performance is shown in Table 1, and a plot comparing ÆGIS to other missions is shown in Figure 4. With such resolution and effective area, ÆGIS will be in a position to address a number of fundamental astrophysical questions, including: *How does Large Scale Structure evolve? Under what conditions do small mass black holes form? What is the behavior of matter at high densities? What role do rotation and magnetic fields play in stellar evolution?*

Figure 5 is a schematic showing the principal components of the spectrometer. Photons from a distant source are focused by a 4.4 m focal length Wolter-I optic that consists of 63 concentric gold-coated mirror shells with radii ranging from 460 to 930 mm. The half power diameter (HPD) of the mirror PSF at the focal point is assumed to be no greater than 10 arc-seconds at 1 keV.

Twelve 30 degree sectors of Critical Angle Transmission (CAT) gratings are located directly behind the optic covering its exit aperture. The gratings in diametric pairs of sectors are arranged such that diffraction from them takes place in the plane that contains the optical axis and is symmetric with respect to the pair. Each pair of opposing grating sectors has its own CCD readout array that detects the diffracted photons. For the six opposing pairs, there are six such symmetry planes, and a total of six CCD readout arrays. There is also a separate CCD camera for detecting the undiffracted (0th-order) photons whose locations are used to provide the origin of the wavelength scale. The zeroth order CCD also provides ÆGIS with some imaging capability.

Parameter	Value	Units	Remarks
Effective area	1440	cm^2	@O VIII Lyα (0.653 keV)
	> 800	cm^2	0.25 - 0.9 keV
$E/\Delta E$	> 3500		0.25 - 2 keV
Focal Length	4.4	m	63 Wolter-I mirror shells
HPD (on-axis)	10	arcsec	
Grating Periods	2000, 2300	Å	arranged in opposing pairs
Blaze Angle	3.5	deg	
Number of CCDs	25		4 per sector pair + 1 for 0th order
CCD Size	25 by 25	mm	24 μm pixels

Table 1. Performance and design parameters for the baseline ÆGIS mission based upon current best estimates.

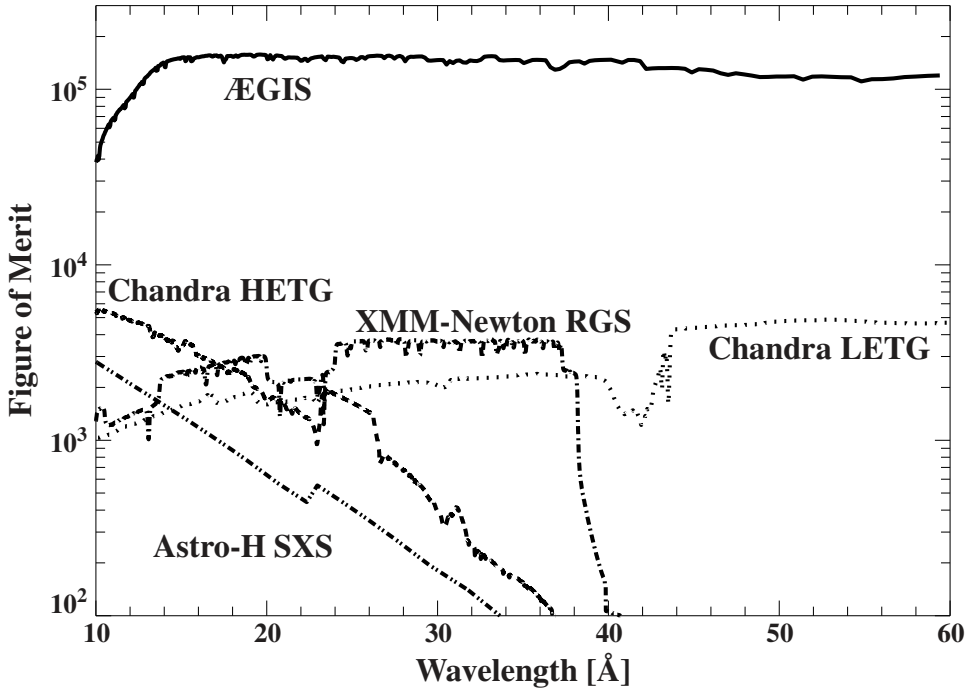

Figure 4. A comparison of ÆGIS to current X-ray observatories. Plotted here is the so-called "figure of merit", which indicates the accuracy of line centroid (and thus velocity) measurement. Its value is equal to the product of the intrument's resolving power and the square root of its effective area ($\mathcal{R}\sqrt{A}$).

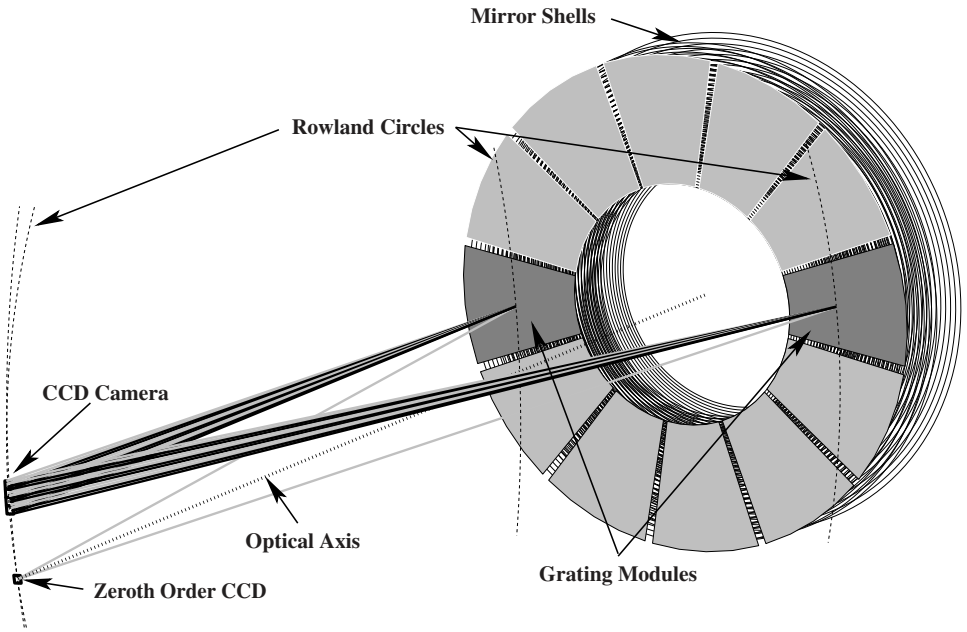

Figure 5. A schematic of the spectrometer for one pair of CAT grating sectors proposed for ÆGIS. A single spectrometer is composed of two diametrically opposite sectors of gratings that diffract to a specctroscopic read-out camera consisting of 4 CCDs. To completely cover the mirror, there will be a total of 6 such spectrometers, and a single shared camera for imaging zeroth order diffracted photons.

A single CCD array consists of four backside-illuminated frame-transfer CCD detectors with a 50-80 eV energy resolution, which is large enough to distinguish overlapping diffraction orders ("order-sorting"). Each CCD in an array is positioned to lie close to the surface of the so-called Rowland torus that contains the zeroth order focus and the associated pair of grating sectors. The distance between the zeroth order location and the point where the torus intersects the optical axis is 4.175 m.

The reason for having six effectively separate spectrometers is to exploit what is called the sub-aperturing effect.[18] Consider, for instance, the horizontal pair of grating sectors that are highlighted in Figure 5. As the figure illustrates, the gratings in those sectors are arranged such that diffraction will take place in a vertical dispersion direction. It is well known that, for sufficiently smooth surfaces, grazing incidence photons will reflect mainly in the plane of incidence with an out-of-plane to in-plane scattering ratio that scales as the sine of the grazing angle. This means that those vertically diffracted photons will have a larger scattering component in the horizontal direction than in the vertical. Stated another way, the mirror scattering will be smaller along the vertical dispersion direction than in the horizontal cross-dispersion direction, and as a result, produce a narrower Line Spread Function (LSF) than it would otherwise (see Figure 6). The sub-aperturing effect plays a critical role in this design, and more will be said about it in the next section.

5. RAYTRACING ÆGIS

The ÆGIS flight mirror assembly was designed to have a 4.4 meter focal length with mirror shell radii running from 460 to 930 mm. These and other geometric constraints were fed to a Wolter-I design program to produce a mirror definition file in the appropriate format for the `marx` Wolter-I mirror module. The result was a file containing all the required parameters to raytrace the mirror, including the required number of shells and their conic parameters. For ÆGIS, this produced a mirror model consisting of 63 gold-coated shells. Henke data tables[19] for gold were used for the reflectivity calculations.

New grating and detector raytrace modules were written for a single pair of CAT grating sectors and its associated CCD spectroscopic array. Both the gratings and the CCDs were arranged to lie close to the surface of a Rowland torus tilted with respect to the optical axis by 1.75 degrees (half of the CAT grating blaze angle).

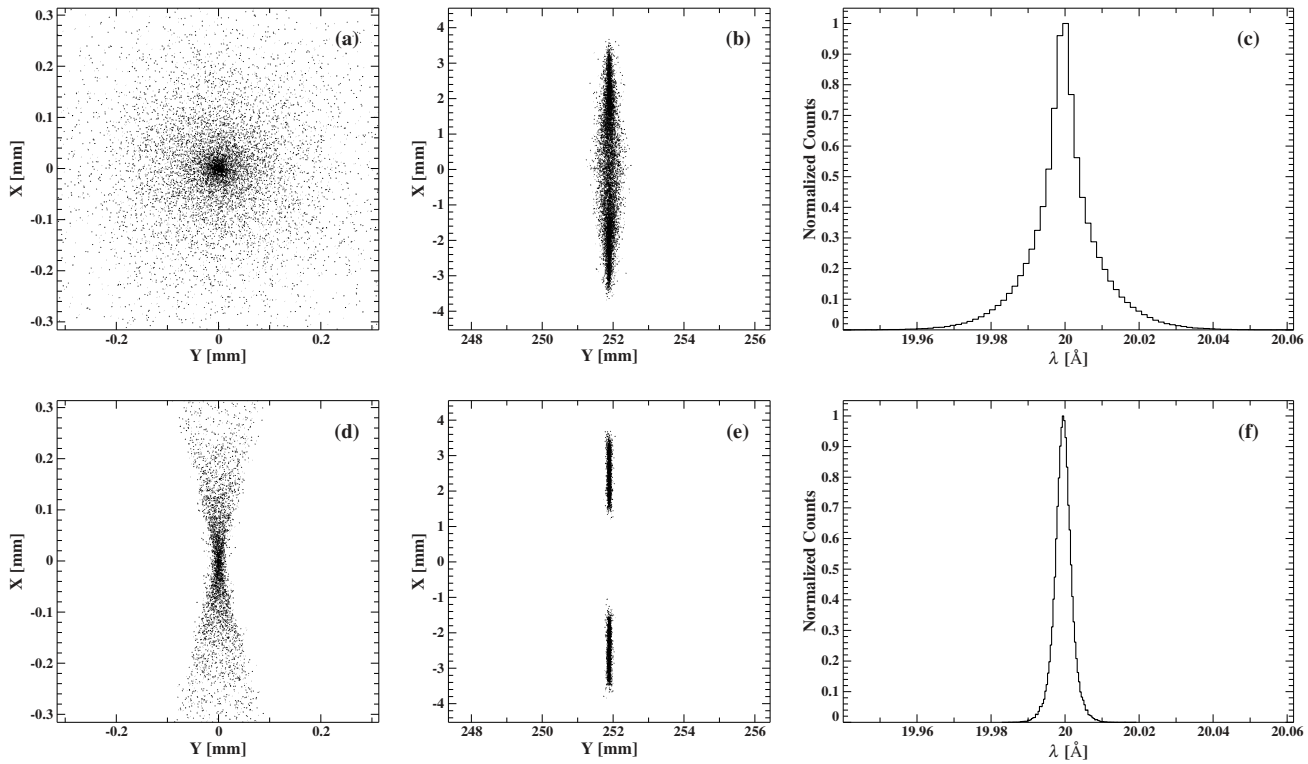

Figure 6. The sub-aperture effect. The plots at the top (a,b,c) were constructed from photons from the full 360 degree mirror, while those at the bottom (d,e,f) were generated from photons from two diametrically opposite 30 degree sectors. The spot diagrams on the left (a,d) represent the 2d PSF in the absence of gratings for the full and sub-apertured cases, respectively. The two middle plots (b,e) correspond to the 2d diffracted events from a 20Å line in 6th order, and the plots on the right (c,f) are the corresponding 1d LSFs. The gap in the spot diagram of the sub-apertured diffracted events (e) is caused by the separation, in the detector plane, of the Rowland circles that pass through the opposing grating sectors. There is no corresponding gap in (b) since the Rowland circles that pass through the gap intersect other gratings outside the sub-aperture. For simplicity, a single grating period (2000Å) was used for the simulations represented here. However, ÆGIS will use 2000Å gratings for one 30 degree sector, and 2300Å gratings for the opposing one. This will cause a shift in one of the two clusters of points in (e) along the dispersion direction (Y axis).

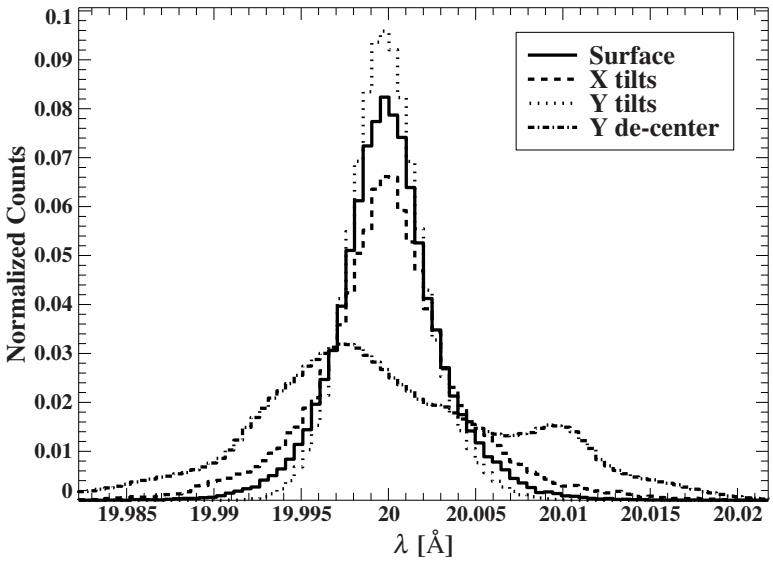

Figure 7. Figure showing the impact of mirror shell surface error and misalignments on the sub-apertured LSF for a 20Å line in sixth order. For clarity, the LSFs for the defocus and X de-center aberrations are not shown because they produce LSFs that differ little from the LSF from Surface effects.

Before the tilting operation, the torus was first rotated about the optical axis by the clocking angle of the sector pair. The size of the torus was chosen such that the distance from the zeroth order focus to the point where the torus meets the optical axis closest to the mirror assembly is 4200 mm. The advantage of this layout is that it gives the all of the grating facets in the sector pair the same orientation with respect to the local incoming photon directions, and minimizes the aberrations associated with the finite facet size.

The energy resolution of the spectrometer is influenced by a number of factors, including the mirror PSF, grating facet size, period errors, CCD pixel size, and system misalignments. As mentioned in the previous section, the size of the mirror PSF in the dispersion direction can be made small by sub-aperturing. In order to fully exploit this effect, it is important to understand how the sub-apertured PSF depends on the various terms that determine the mirror PSF. For our investigation, we assumed that the 10 arc-second half-power diameter PSF resulted solely from a single type of aberration. We then raytraced the various types in turn to see which ones have the strongest influence upon the sub-apertured PSF. In particular, we considered separately the following blurs:

Surface blur : A blur stemming from random deviations of the surface normals with respect to the idealized normals. This was used as a proxy for mirror scatter and figure error ($\sigma = 4''$).

X tilts : Random rotations of the shells about the X axis ($\sigma = 4.9''$)

Y tilts : Random rotations of the shells about the Y axis ($\sigma = 4.9''$)

Defocus : Random displacements of the shells along the optical axis ($\sigma = 0.8$ mm).

X de-center : Random displacements of the shells along the X axis ($\sigma = 0.13$ mm)

Y de-center : Random displacements of the shells along the Y axis ($\sigma = 0.13$ mm)

Here, the X axis lies in cross-dispersion direction, the Y axis is in the dispersion direction, and for each type of aberration, random deviates were sampled from a Gaussian distribution whose σ was adjusted to give a PSF with a $10''$ HPD.

As Figure 7 shows, the LSF is quite sensitive to the de-centers of the mirror shells along the Y axis. This is to be expected since the Y axis is parallel to the dispersion axis and any shifts of the mirror shells along the

dispersion direction will directly affect the width of the LSF. In addition, this figure also shows that the LSF is affected by tilts of the shells about the X axis, but not nearly as much as displacements along the Y axis. From these simulations we see that in order for the sub-aperturing effect to be realizable in practice, it is important to have much tighter tolerances on the de-centers along the dispersion direction than in the cross-dispersion direction.

6. SUMMARY

In this paper, we described the role that the **MARX** raytrace program plays in connection with the Chandra X-ray observatory. We reviewed some of its evolution within the project from a program that provided simple simulated event data for the development and testing of grating pipelines to sophisticated simulated observations of our Galactic center.

We have also shown how we adapted **MARX** to facilitate the design of a future X-ray observatories. It has been indispensable for testing various ÆGIS spectrometer designs and for making realistic predictions of the performance of ÆGIS, as well as for other proposed concepts such as IXO and AXSIO. Based upon our experience with **MARX** within the Chandra mission, we expect that **MARX** will play a similar role in the context of a new X-ray observatory mission.

ACKNOWLEDGMENTS

We would like to take this opportunity to thank two individuals that played important roles in the early stages of the development of **MARX**: Michael Wise for his work in testing and documenting much of the raytrace, as well as his insistence that it be user friendly, and Kazunori "Bish" Ishibashi for his hard work in the calibration of the **MARX** LSFs. This work was supported by NASA through the Smithsonian Astrophysical Observatory (SAO) contract SV3-73016 to MIT for support of the CXC and Science Instruments; the CXC is operated by SAO for and on behalf of NASA under contract NAS8-03060. RKH and MLS acknowledge support from NASA grant NNX11AF30G, and RKS acknowledges support from NASA grant NNX08AB46A.

REFERENCES

[1] Wise, M. W., Huenemoerder, D. P., and Davis, J. E., "Simulated AXAF Observations with MARX," in [*ASP Conf. Ser. 216: Astronomical Data Analysis Software and Systems VI*], **125**, 447–480 (1997).

[2] Weisskopf, M. C., Brinkman, B., Canizares, C., Garmire, G., Murray, S., and Van Speybroeck, L. P., "An Overview of the Performance and Scientific Results from the Chandra X-Ray Observatory," *Publ. Astron. Soc. Pac.* **114**, 1–24 (Jan. 2002).

[3] Weisskopf, M. C., Aldcroft, T. L., Bautz, M., Cameron, R. A., Dewey, D., Drake, J. J., Grant, C. E., Marshall, H. L., and Murray, S. S., "An Overview of the Performance of the Chandra X-ray Observatory," *Experimental Astronomy* **16**, 1–68 (Aug. 2003).

[4] Stage, M. D. and Dewey, D., "Verifying the HETG spectrometer Rowland design," in [*Society of Photo-Optical Instrumentation Engineers (SPIE) Conference Series*], Hoover, R. B. and Walker, A. B., eds., *Society of Photo-Optical Instrumentation Engineers (SPIE) Conference Series* **3444**, 36–47 (Nov. 1998).

[5] Primini, F. A., Houck, J. C., Davis, J. E., Nowak, M. A., Evans, I. N., Glotfelty, K. J., Anderson, C. S., Bonaventura, N. R., Chen, J. C., Doe, S. M., Evans, J. D., Fabbiano, G., Galle, E. C., Gibbs, D. G., Grier, J. D., Hain, R. M., Hall, D. M., Harbo, P. N., (Helen He, X., Karovska, M., Kashyap, V. L., Lauer, J., McCollough, M. L., McDowell, J. C., Miller, J. B., Mitschang, A. W., Morgan, D. L., Mossman, A. E., Nichols, J. S., Plummer, D. A., Refsdal, B. L., Rots, A. H., Siemiginowska, A., Sundheim, B. A., Tibbetts, M. S., Van Stone, D. W., Winkelman, S. L., and Zografou, P., "Statistical Characterization of the Chandra Source Catalog," *Astrophys. J., Suppl. Ser.* **194**, 37 (June 2011).

[6] Heilmann, R. K., Davis, J. E., Dewey, D., Bautz, M. W., Foster, R., Bruccoleri, A., Mukherjee, P., Robinson, D., Huenemoerder, D. P., Marshall, H. L., Schattenburg, M. L., Schulz, N. S., Guo, L. J., Kaplan, A. F., and Schweickart, R. B., "Critical-Angle Transmission Grating Spectrometer for High-Resolution Soft X-Ray Spectroscopy on the International X-Ray Observatory," in [*Space Telescopes and Instrumentation 2010: Ultraviolet to Gamma Ray*], Arnaud, M., Murray, S. S., and Takahashi, T., eds., *Proc. SPIE* **7732**, 77321J (2010).

[7] Bookbinder, J., "The International X-ray Observatory - RFI#2," *ArXiv e-prints, 1003.2847* (Mar. 2010).
[8] Bookbinder, J., "The Advanced X-ray Spectroscopic Imaging Observatory," RFI/NNH11ZDA018L: Mission Concepts for X-ray Astronomy, NASA (2011).
[9] Bautz, M. W., Allen, G. E., Bookbinder, J., Bregman, J., Brickhouse, N., Burrows, D. N., Canizares, C. R., Chakrabarty, D., Chan, K.-W., Davis, J. E., Dewey, D., Drake, J. J., Elvis, M. S., Evans, D., Falcone, A., Flanagan, K., Heilmann, R., Houck, J. C., Huenemoerder, D. P., Jordan, S., Lee, J. C., Loewenstein, M., Marshall, H. L., Mathur, S., Miller, J. M., McClelland, R. S., Mushotzky, R., Nicastro, F., Nowak, M. A., O'Dell, S., Paerels, F., Petre, R., Ptak, A., Saha, T. T., Schattenburg, M., Schulz, N., Smith, R. K., Wang, D., Wolk, S., and Zhang, W. W., "AEGIS— An Astrophysics Experiment for Grating and Imaging Spectroscopy," RFI/NNH11ZDA018L: Mission Concepts for X-ray Astronomy, NASA (2011).
[10] Canizares, C. R., Davis, J. E., Dewey, D., Flanagan, K. A., Galton, E. B., Huenemoerder, D. P., Ishibashi, K., Markert, T. H., Marshall, H. L., McGuirk, M., Schattenburg, M. L., Schulz, N. S., Smith, H. I., and Wise, M., "The Chandra High-Energy Transmission Grating: Design, Fabrication, Ground Calibration, and 5 Years in Flight," *Publ. Astron. Soc. Pac.* **117**, 1144–1171 (Oct. 2005).
[11] Davis, J. E., "Event Pileup in Charge-coupled Devices," *Astrophys. J.* **562**, 575–582 (Nov. 2001).
[12] Davis, J. E., "The Formal Underpinnings of the Response Functions Used in X-Ray Spectral Analysis," *Astrophys. J.* **548**, 1010–1019 (Feb. 2001).
[13] Houck, J. C. and Denicola, L. A., "ISIS: An Interactive Spectral Interpretation System for High Resolution X-Ray Spectroscopy," in [*ASP Conf. Ser. 216: Astronomical Data Analysis Software and Systems IX*], **9**, 591+ (2000).
[14] Ishibashi, K., Dewey, D., Huenemoerder, D. P., and Testa, P., "Chandra/HETGS Observations of the Capella System: The Primary as a Dominating X-Ray Source," *Astrophys. J., Lett.* **644**, L117–L120 (June 2006).
[15] Marshall, H. L., Dewey, D., and Ishibashi, K., "In-flight calibration of the Chandra high-energy transmission grating spectrometer," in [*Society of Photo-Optical Instrumentation Engineers (SPIE) Conference Series*], Flanagan, K. A. and Siegmund, O. H. W., eds., *Society of Photo-Optical Instrumentation Engineers (SPIE) Conference Series* **5165**, 457–468 (Feb. 2004).
[16] Jerius, D. H., Cohen, L., Edgar, R. J., Freeman, M., Gaetz, T. J., Hughes, J. P., Nguyen, D., Podgorski, W. A., Tibbetts, M., Van Speybroeck, L. P., and Zhao, P., "The role of modeling in the calibration of the Chandra's optics," in [*Society of Photo-Optical Instrumentation Engineers (SPIE) Conference Series*], Flanagan, K. A. and Siegmund, O. H. W., eds., *Society of Photo-Optical Instrumentation Engineers (SPIE) Conference Series* **5165**, 402–410 (Feb. 2004).
[17] Pelupessy, F. I., Schaap, W. E., and van de Weygaert, R., "Density estimators in particle hydrodynamics. DTFE versus regular SPH," *Astron. Astrophys.* **403**, 389–398 (May 2003).
[18] Cash, Jr., W. C., "X-ray optics. II - A technique for high resolution spectroscopy," *Appl. Opt.* **30**, 1749–1759 (May 1991).
[19] Henke, B. L., , Gullikson, E. M., and Davis, J. C., "X-ray interactions: photoabsorption, scattering, transmission, and reflection at e=50-30000 ev, z=1-92," *Atomic Data and Nuclear Data Tables* **54**(2), 181–342 (1993).